Marine Biology 113, 319–328 (1992)

Marine Biology
International Journal on Life in Oceans and Coastal Waters

Comparison of sinking velocity, swimming velocity, rotation and path characteristics among six marine dinoflagellate species

D. Kamykowski [1], R. E. Reed [1] and G. J. Kirkpatrick [2]

[1] Department of Marine, Earth and Atmospheric Sciences, North Carolina State University, Raleigh, North Carolina 27695-8202, USA
[2] Mote Marine Laboratory, 1600 Thompson Parkway, Sarasota, Florida 34236, USA

Date of final manuscript acceptance: January 17, 1992. Communicated by J. M. Lawrence, Tampa

Abstract. Six marine dinoflagellate species representing a range of equivalent spherical diameters between 12 and 36 μm were examined for several characteristics that influence their translation velocity. Sinking velocities estimated by three independent techniques and applied to swimming and narcotized cells generally agreed, and followed the cell-size relationships previously reported for diatoms. Dinokont sinking and swimming velocities both decreased with increasing surface area:volume ratio, but a small desmokont deviated from the dinokont relationships. Sinking velocities influenced the relative ascent/descent capabilities of a species. The swim:sink ratio decreased as equivalent spherical diameter increased to 25 μm and then remained constant at 7.6, despite further increases in cell size. This relationship suggests a minimum required swimming capability relative to cell size. The swim:sink ratio increased with increasing surface area:volume ratio for all the surveyed species. Our observations of decreasing cell rotation:translation ratio and increasing cell drag with increasing cell size supported the hypothesis that the dinoflagellate flagellar apparatus generates maximum swimming velocity at intermediate cell sizes. However, an alternate analysis supported the hypothesis that swimming velocity increases with cell size and that variations among genera are due to subtle differences in the basic dinoflagellate propulsion system. A three-dimensional helical path index provided a more realistic estimate of the actual translation velocity (along the helix axis) during diel vertical migration when applied as a correction factor to the more typically measured helix velocity (along the helix) of a given dinoflagellate.

Introduction

Most classes of marine phytoplankton are motile (Cox 1980). Of these motile classes, dinoflagellates are among the best known because of their unusually large size range (between 2 μm and 2 mm in length, with the majority between 20 and 200 μm) and because of their abundance in coastal areas (Taylor and Pollingher 1987). Although many aspects of dinoflagellate motility have been investigated (Levandowsky and Kaneta 1987), the ecological understanding of this capability remains incomplete.

Smayda (1970) included only one dinoflagellate, *Gonyaulax polyedra* measured by Eppley et al. (1967), in his review of phytoplankton sinking velocity. This lack of emphasis is understandable, based on the reasoning that swimming capability makes sinking velocity less interesting. Two observations, however, support the necessity of a more thorough study of dinoflagellate sinking velocities. First, Kamykowski and McCollum (1986) identified a highly variable, but possibly significant, size-dependence of dinoflagellate swimming velocity, such that intermediate-sized species appear to exhibit the fastest swimming velocities. Since sinking velocity increases with the square of the radius according to Stokes' law, larger dinoflagellates may combine relatively slow swimming velocities with relatively large sinking velocities. Kamykowski et al. (1989) speculated on this relationship, but their sinking-velocity data were based on very generalized computations of Stokes' law. Second, Kamykowski et al. (1988) presented laboratory data that supported Robert's (1981) contention that a species' descent velocity exceeds its ascent velocity by twice the sinking velocity under constant environmental conditions. This rate difference may be especially significant for larger dinoflagellates with relatively high sinking velocities and may translate into a diel vertical migration distance or scope that is determined by the slower ascent velocity.

Levandowsky and Kaneta (1987) stated that most dinokonts swim along a clockwise helical path [they use the term "spiral", but helical is more correct (Bovee 1982)] with the sulcus usually facing the axis of the helix (e.g. Peters 1929). They further stated that the helical path is thought to stabilize the direction of motion; some large, slow-swimming species that do not follow a helix tend to rock as they swim. In a typical dinokont, the helical path is often attributed to direct action of the transverse flag-

ellum or to a helical beating pattern of the longitudinal flagellum, but other evidence associates cell morphology with helical swimming (Levandowsky and Kaneta 1987). Bovee (1982) reported that different euglenoid species exhibit different helix radii; species with very small helix radii essentially rotate as they swim.

Brennen and Winet (1977) and Roberts (1981) suggested that enhanced cell rotation due to small cell size can reduce translation velocity compared to somewhat larger cell sizes. Kamykowski and McCollum (1986) invoked this mechanism to explain the apparent decrease in swimming velocity below equivalent spherical diameters (ESDs) of ~35 μm. Brennen and Winet (1977) and Roberts (1981) also suggested that although increasing cell size retards rotation and thus can contribute to more efficient translation, the simultaneously increasing drag (Happel and Brenner 1983) can contribute to reduced translation velocity at sufficiently large cell sizes. Kamykowski and McCollum (1986) invoked this latter mechanism to explain the apparent decrease in swimming velocities at larger cell sizes above ESDs of ~35 μm. This hypothesis of an intermediate dinoflagellate cell size for maximum swimming velocity is in contrast to the more typical direct relationship between swimming velocity and cell length discussed by Okubo (1987).

Helical swimming is one component of the overall path that a species follows (Levandowsky and Kaneta 1987, Crenshaw 1990). In the remainder of this paper, the exact three-dimensional path followed by a cell is referred to as the "helix distance", while the distance along the helix axis is referred to as the "translational distance" [see Fig. 10.2 in Levandowsky and Kaneta (1987)]. Velocity follows a parallel terminology. Some species may exhibit a more erratic component that appears when a cell frequently changes its mean direction. This type of behavior may result from differential sensitivity among species to any of a number of sensory cues (Levandowsky and Kaneta 1987). Crenshaw (1990) speculated on the sensory advantages of a helical swimming motion.

The present paper extends the previous discussion by examining dinoflagellate sinking velocity and swimming velocity in more detail. It also provides new interspecies comparisons of cell rotation, cell drag, two computer-derived path characteristics (net-to-gross displacement and rate-of-change-of-direction), and a geometrically derived, three-dimensional helical path index.

Materials and methods

Cultures

Unialgal cultures of six dinoflagellate species – *Prorocentrum mariae-lebouriae* (Parke and Ballentine) Faust (from Dr. M. Altalo) (*Proro*); *Scrippsiella trochoidea* (Stein) Loeblich (Clone CCMP1331 from the Bigelow Marine Laboratory) (*Scripps*); *Peridinium foliaceum* (Stein) Biecheler (from Dr. M. Huntley) (*Perid*); *Gymnodinium sanguineum* Hirasaka (Clone CCMP 417; also known as *Gymnodinium splendens*) (*Gymno*); *Gyrodinium dorsum* Kofoid (from Dr. M. Huntley) (*Gyro*); and *Gonyaulax polyedra* Stein (Clone CCMP405) (*Gonyau*) – were grown in *f*/2 media without silicic acid at 30‰ in 1-liter glass cylinders (58 mm diam × 440 mm height). The bottom third of the cylinder was covered with black plastic, the middle third with neutral screening material (60% transparency), and the top was left clear. Cultures were maintained at 20 °C ± 1 C° under a 12 h light:12 h dark cycle using cool-white fluorescent illumination providing 150 μmol m^{-2} s^{-1} PAR (photosynthetically active radiation). When an experiment was conducted, a bulk sample was taken from the clear portion of the cylinder at 11.00 hrs to focus on an actively migrating, nutrient-replete ("healthy" vs nutrient-deplete or "senescent") subpopulation and was divided into subsamples for each determination. The subsamples were kept in a growth chamber at the same light intensity and temperature as the column culture. The one exception was that the cells examined for rotation:translation ration were obtained directly from stock cultures.

The selected dinoflagellates included one relatively small desmokont that approximated an oblate spheroid with an ESD of 11.5 μm and five dinokonts dominated by prolate spheroids with ESDs ranging from 22 to 36 μm. *Gymnodinium sanguineum* was treated uniquely as a geometric construction formed by the arrangement of three cones and a cylinder because of its complex shape (Bailey 1975). Among the dinokonts, only *G. sanguineum* and *Gyrodinium dorsum* are considered athecate [however, some gymnodinoid species possess a delicate theca (Taylor 1987)].

Narcotization of cells

Sinking-velocity determinations were performed on normal swimming cells and on narcotized cells (irregular flagellar beating with no directed motion by the cell). Trials with the known narcotizing agents MS-222 (tricaine methanesulphonate from the Sandoz Chemical Co.), and menthol crystals, and with two types of nicotine solutions (pure nicotine dissolved in filtered seawater from Sigma Chemical Co. and a solution made by leaching spent mentholated cigarette filters in seawater) after Omori and Ikeda (1984), and EDTA/oxalic acid after Lindholm (1982) revealed that the seawater/filter extract produced the most uniform narcotization without detectable cellular damage. The other agents used, even various concentrations of the pure nicotine, caused shrinking or swelling that led to obvious loss of viability. Two of the species were not amenable to any narcotization method tried: *Gymnodinium sanguineum* exhibited cellular swelling and breakage and *Gonyaulax polyedra* underwent ecdysis and became rounded and swollen.

Filter-fibers were taken from five smoked menthol-filtered cigarettes and were soaked in 20 ml filtered seawater overnight. The resulting liquid was then filtered through a GF/F filter (Whatman) and stored at room temperature in a foil-covered container. Fresh, mentholated, nicotine solution was made-up for each experiment. Since the susceptibility of different species to narcotization varied, experiments were performed to standardize the response to the solution. The extract was added dropwise to 10 ml of dinoflagellate culture until ~20% of the cells were narcotized. This concentration produced 90% narcotization in 30 min with the species that we found susceptible.

Fluorometric sinking rate determinations

A Turner Designs fluorometer, equipped with a water-jacketed curvette holder set at 20 °C, and a Weathermeasure chart recorder were used to determine dinoflagellate sinking velocities. The modified homogeneous sample method of Bienfang et al. (1977) required fluorometer sinking-rate tubes constructed by placing a silicon-rubber stopper in the bottom of a fluorometer cuvette and isolating a 1 cm light path above the stopper by blackening the area below the top of the stopper and 1 cm above the top of the stopper with opaque tape. For sinking-rate determinations, three 10 ml subsamples were used. These samples were left in the incubator after collection from the growth column at the light intensity equal to the top of the column. From the 10 ml sample, 2 ml of culture were placed into the sinking-rate tubes and then into a dark box in the incubator for 2 min to allow dark equilibration. The tube was then removed

from the box, gently inverted twice to mix, and then immediately placed into the fluorometer for sinking-rate determination. Temperature equilibration was required to eliminate any motion due to convection. The fluorometric sinking velocities (V_i) were calculated according to

$$V_i = (\Delta\text{fluor}/\Delta\text{time})\,(\text{initial fluor})\,. \quad (1)$$

Stokes' law: sinking-velocity determinations

Assuming low Reynolds numbers (see "Discussion – Reynolds numbers"), the calculation of complete Stokes' law sinking velocities (V_i), according to

$$V_i = 2gr^2(\varrho_0 - \varrho_w)/9\mu\phi\,, \quad (2)$$

where g = acceleration of gravity, required estimates of cell density (ϱ_0), radius (r), shape factor (ϕ), seawater density (ϱ_w) and viscosity (μ). Cell density was obtained by NaCl-adjusted, iso-osmotic Percoll (Pharmacia, Uppsala, Sweden) and $f/2$-media density-gradients adapted from the method of Van Ierland and Peperzak (1984). A linear density gradient was formed in a polycarbonate centrifuge tube to a final volume of 35 ml using the two-cylinder approach described by Price (1972). An 8 ml dinoflagellate sample was overlayed gently on the gradient and then centrifuged at 2250 $\times g$ for 25 min. By slowly accelerating and decelerating the centrifuge rotor to and from the equilibrium velocity, care was taken not to disturb the gradient. The gradient was fractionated into 2 ml fractions over a 10 min interval using an ISCO gradient fractionator and a fraction collector in subdued light. Relative fluorescence in a Turner Designs fluorometer and refractive index with a handheld American Optical Corporation refractometer were determined on each 2 ml fraction to locate the highest concentration of cells and their settled density. Red density-marker beads (1.110 g cm^{-3}; Pharmacia, Uppsala, Sweden) were included in each run as the endpoint determinations of the linear density-gradient. The refractive index was used as a check for linearity in the gradients. The top of the density gradient was 1.021 g cm^{-3}, the density of the $f/2$ media; the bottom of the density gradient was 1.131 g cm^{-3}, the density of the NaCl-adjusted Percoll. A graph of fluorescence without cells as a function of the density of each fraction provided a blank curve. Fluorescence with cells was then determined for each species, the blank curve was subtracted, and a residual fluorescence represented the species' distribution in the density gradient. The mean and standard deviation of each species' density were determined by plotting the cumulative percent of the residual fluorescence as a function of density on normal probability paper.

The cell radius for the Stokes' law calculation was obtained from Coulter counter volume-estimates and from microscope measurements of the dinoflagellate cells. In the former case, Coulter volumes were determined using the standard procedures (Parsons et al. 1984) with a Coulter Zb Counter. Coulter diameters were calculated from an assumed spherical approximation. In the latter case, the length (l or L), width (w), and/or height (h) axes were measured on tens of cells using a Nikon Diaphot inverted microscope calibrated with a stage micrometer. Measurements on cells with two equal dimensions as determined from a survey of settled cells were performed on narcotized cells. Cells with three unequal dimensions were suspended in agarose (Reize and Melkonian 1989) to allow visualization of all three axes, but only two axes were measured on any one cell. The microscope measurements were used to calculate ESD [$d = (l\,w\,h)^{1/3}$], eccentricity [$\varepsilon = c/a$, where a is the major axis and $c = (a^2 - b^2)^{1/2}$, where b is the minor axis], shape factor (McNown and Malaika 1950), and surface area (SA) and volume (V) based on one of the two types of spheroids (Selby 1965) applicable to each species [except *Gymnodinium sanguineum*, for which we utilized a corrected version of Bailey's (1975) approach]. SAS analysis (SAS Institute Inc. 1985) or the error propagation method of Rees (1984) were used to determine the mean, standard deviation, variance and covariance components. Seawater density and seawater viscosity were obtained from tables of the U.S. Navy Oceanographic Office (1966).

Video swimming and sinking-velocity determinations

A video system consisting of a Dage-MTI CCD 72 camera, a monitor, and a Panasonic studio-grade VCR coupled to a Wild dissecting scope was used to video-tape the swimming velocity (V_w) and the sinking velocity (V_i) of swimming and narcotized cells in a vertical plane. A subpopulation was placed in a water-jacketed cuvette set at 20 °C and illuminated from above with PAR at the experimental light intensity and from the side with the infrared source. The raw footage obtained after convection subsided was analyzed using the Motion Analysis Corporation "Expertvision" motion-analysis system (Kamykowski et al. 1988) after selecting every sixth frame from a recording made at 30 frames s^{-1}. For swimming velocity, the overall population was considered irrespective of swimming direction. For sinking velocity on swimming cells, the overall population was divided into ascending and descending subpopulations using the software editor, and average sinking velocity was calculated according to Roberts (1981) from

$$V_i = (\text{descent } V_w - \text{ascent } V_w)/2\,. \quad (3)$$

All the terms in this equation represent population averages. For sinking velocity on narcotized cells, the population was measured directly.

Rotation/translation determinations

Additional populations from dinoflagellate stock cultures were videotaped using a Nikon-Diaphot inverted-microscope equipped with a 0 to 2.25× zoom lens coupled to a Dage-MTI CCD 72 video-camera illuminated with the microscope light. Distance was determined by calibration with a Wild stage-micrometer and rotation was determined by visual analysis of slow-motion video-replay using a Panasonic studio-grade VCR. Cellular radii were taken directly from the monitor screen (characterized by low edge-distortion) and converted into micrometers using the calibration values. *Scrippsiella trochoidea* was not examined due to the absence of cellular features to support the visual discrimination of rotation. The routine measurement consisted of measuring the net distance traveled relative to a quarter turn (*Gymnodinium sanguineum*), a half turn (*Prorocentrum mariae-lebouriae* and *Gonyaulax polyedra*) or a whole turn (*Peridinium foliaceum* and *Gyrodinium dorsum*). The net distance traveled is treated as an approximation to the translation distance and not the helix distance. The accuracy of this approximation varies with the path characteristics of the different species.

Reynolds number (Re) was calculated using the formula

$$Re = \varrho_w\,Ur/\mu\,, \quad (4)$$

and drag (F) using the formula,

$$F = 6\pi\,\mu\,r\,U\,, \quad (5)$$

where ϱ_w is the water density, U is the translation velocity, r is the appropriate radius of the cell, and μ is the water viscosity (Happel and Brenner 1983). Units were adjusted to accommodate the calculation.

Path characteristics

The same video-tapes used for the swimming-velocity determinations were surveyed for representative two-dimensional paths. The depth of focus of the microscope system combined with the operating characteristics of the motion analysis system to transform the three-dimensional motion of the cells to a two-dimensional plane. These paths were re-analyzed for net-to-gross displacement (NGD) and rate-of-change-of-direction (RCD) using the "Expertvision" motion-analysis system. NGD is an index of path twistedness or convolution. In the simplest case, a straight path gives an NGD value of 1 and a closed circular path gives a value of 0. RCD is an

index of turning rate regardless of direction, and is measured as the absolute value of the angular velocity. The histogram presentation of the results (see "Discussion – Path characteristics") is strongly biased toward the zero degree location for cells that swim in nearly straight paths, and is more uniformly distributed between 0 and 180° for cells that continuously change direction.

The helical swimming paths for the different species were characterized by measuring the helix diameter and the length of one helix cycle for several cells from the same video-tapes used for the swimming-velocity determinations. The measurements were made on the video screen (characterized by low edge-distortion) with a metric rule calibrated to the scale of the video image by means of a stage micrometer. These measurements were used to calculate the three-dimensional length of the helical distance (H; μm) from

$$H = 2\pi(a^2 + b'^2)^{1/2}, \quad (6)$$

where a (μm) is the helix radius and b' (μm rad^{-1}) is the length of one helix cycle (b; μm) divided by 2π after Salas and Hille (1974). Considering the null cases, when $a=0$, then $H=b$ or the cell swims in a straight line without helical motion; when $b=0$, then $H=2\pi a$ or the cell swims in a circle with radius "a" in the horizontal plane. The pattern for each species is reported as the helical path index (HPI), the ratio of the length of one helix cycle (or the translation distance that is related to the translation velocity) divided by the length of the helical path (or the helix distance that is related to the helix velocity). Crenshaw (1990) provided a more complete discussion of the kinetics of helical motion as applied to sperm and some microorganisms.

Results

General cell characteristics

Table 1 summarizes the various cell characteristics basic to the study of sinking velocity and swimming style for the six selected marine dinoflagellate species. The species (*Gyro* I and II positioned in Table 1 by *Gyro* I value are listed according to increasing ESD from left to right (a–g). Two different subcultures of the same clone of *Gyrodinium dorsum* (*Gyro* I and *Gyro* II) were measured for most of the attributes about one month apart to examine the reproducibility of the various techniques. The densities of all the selected species are significantly greater than that of the seawater medium (~1.021 g cm^{-3}). Narcotized cells exhibited a more uniform density range (1.082 to 1.094 g cm^{-3}) compared to swimming cells (1.064 to 1.090 g cm^{-3}), with the greatest differences between treatments among the smaller cells.

Sinking velocity

The seven estimates of sinking velocity based on three independent measurement methods and applied to swimming and narcotized cells are listed in Table 2 and are directly compared in Fig. 1. Both present the species in order of increasing ESD. The missing values for the narcotized cells result from the sensitivity of *Gymnodinium sanguineum* and *Gonyaulax polyedra* to the agents used and to the lack of replication for the density determination of narcotized *Gyrodinium dorsum*. The species lacking video determinations did not provide enough ascending or descending paths to support the calculation. Since the fluorometric approach revealed similar velocities for swimming ("Fluor"; Table 2) and narcotized ("Fluor-n") cells, the presence of swimming cells does not appear to interfere with the technique as described. Comparison of the "Stokes" (calculated without the shape factor) and "Stokes'-sf" rows in Table 2 indicates that shape factor (sf) is not a significant variable for the selected species

Table 1. *Prorocentrum mariae-lebouriae* (*Poro*), *Scrippsiella trochoidea* (*Scripps*), *Peridinium foliaceum* (*Perid*), *Gymnodinium sanguineum* (*Gymno*), *Gyrodinium dorsum* (*Gyro* I and II) and *Gonyaulax polyedra* (*Gonyau*). Summary of cell-specific characteristics. *Gyro* I and II represent measurements made one month apart on same clone. Values are means (±1 SD) in μm, except when stated otherwise. Desmo: desmokont; Dino: dinokont (Taylor 1987). Theca: + = present, − = absent, −(+) = some gymnodinoid species possess delicate theca (Taylor 1987); Equivalent spherical diameter (ESD): $d=(l\,w\,h)^{1/3}$, where l, w and h are cell dimensions; Coulter diam: estimated from spherical approximation; Shape: oblate or prolate spheroids, geometric is more complicated shape (Bailey 1975); Eccentricity: eccentricity from $\varepsilon=c/a$, where a is major axis and $c=(a^2-b^2)^{1/2}$, with b as the minor axis; Shape factor: Stokes' law shape-factor computed after McNown and Malaika (1950); SA:V: surface area:volume ratio; Density: density of motile cells; Density-n: density of cells exposed to nicotine in order to stop swimming activity

Characteristic	*Proro* (a)	*Scripps* (b)	*Perid* (c)	*Gymno* (d)	*Gyro* I (e)	*Gyro* II (f)	*Gonyau* (g)
Flagellar type	Desmo	Dino	Dino	Dino	Dino	Dino	Dino
Theca	+	+	+	−(+)	−	−	+
Length	14.8 (1.7)	25.3 (2.4)	30.6 (3.3)	47.6 (4.0)	37.5 (4.1)	39.4 (2.8)	39.2 (3.7)
Width	14.8 (1.7)	19.9 (2.1)	30.6 (3.3)	30.9 (3.3)	31.3 (3.0)	34.1 (2.4)	33.3 (3.5)
Height	7.3 (1.0)	19.9 (2.1)	18.3 (3.3)	23.2 (2.0)	31.3 (3.0)	34.1 (2.4)	33.3 (3.5)
ESD	11.7 (0.7)	21.6 (1.1)	25.7 (1.5)	32.4 (1.5)	33.2 (1.7)	35.8 (1.3)	35.2 (1.8)
Coulter diam	11.2 (1.4)	20.8 (2.9)	25.2 (3.0)	39.5 (4.5)	30.4 (3.2)	32.4 (3.1)	31.6 (4.5)
Shape	Oblate	Prolate	Oblate	Geometric	Prolate	Prolate	Prolate
Eccentricity	0.87	0.62	0.80	ND	0.55	0.50	0.53
Shape factor	1.071 (0.003)	0.998 (0.001)	1.043 (0.001)	1.088 (0.010)	0.997 (0.001)	0.997 (0.000)	0.997 (0.001)
Surface area (μm^2)	475	1478	2189	4821	3488	4035	3905
Volume (μm^3)	846	5267	8939	18 140	19 216	23 973	22 783
SA:V (μm^{-1})	0.56	0.28	0.25	0.27	0.18	0.17	0.17
Density (g cm^{-3})	1.064 (0.015)	1.077 (0.007)	1.080 (0.012)	1.073 (0.007)	1.090 (0.009)	1.085 (0.004)	1.084 (0.007)
Density-n (g cm^{-3})	1.082 (0.012)	1.086 (0.008)	1.087 (0.013)	ND	1.094 (0.005)	ND	ND

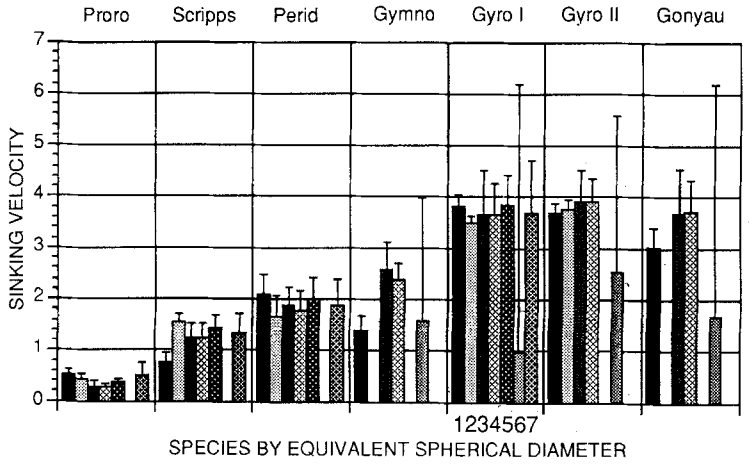

Fig. 1. *Prorocentrum mariae-lebouriae* (*Proro*), *Scrippsiella trochoidea* (*Scripps*), *Peridinium foliaceum* (*Perid*), *Gymnodinium sanguineum* (*Gymno*), *Gyrodinium dorsum* (*Gyro* I and II) and *Gonyaulax polyedra* (*Gonyau*). Comparison of seven different estimates of sinking velocity (m d^{-1}; numbered 1–7 in Table 2). Bars above columns represent one standard deviation. Species arranged in order of increasing equivalent spherical diameter (ESD, Table 1) except for *Gyro* I and II, which are positioned by the *Gyro* I value

Table 2. *Prorocentrum mariae-labouriae* (*Proro*), *Scrippsiella trochoidea* (*Scripps*), *Peridinium foliaceum* (*Perid*), *Gymnodinium sanguineum* (*Gymno*), *Gyrodinium dorsum* (*Gyro* I and II) and *Gonyaulax polyedra* (*Gonyau*). Summary of sinking velocity, swimming velocity, Reynolds number, cell rotation, net-to-gross displacement and helical path index. Values are means (±1 SD). Sink. vel.: sinking velocities at 20 °C, calculated over 24 h day; Fluor: fluorescence technique with swimming cells; Fluor-n: fluorescence technique with cells exposed to nicotine in order to stop swimming activity; Stokes: Stokes' law calculation-technique using equivalent spherical diameters; Stokes'-sf: "Stokes" with shape factor included; Stokes'-n: "Stokes" with cell density determined on nicotine-exposed cells; Video: motion analysis based on one-half the difference between descent and ascent velocities; Video-n: motion analysis based on sinking of nicotine-exposed cells; Swim. vel.: representative horizontal swimming velocities at 20 °C; Sink. Rey no.: Reynolds number based on "Fluor" sinking velocity; Swim. Rey no.: Reynolds number based on swimming velocity; Swim: sink: swimming velocity divided by "Fluor" sinking velocity; Approx rad: approximate equivalent spherical radius from two cell dimensions for cell populations used to determine rotation and translation; $\omega:U$: rotational velocity (ω; rad s^{-1}) divided by translational velocity (U; μm s^{-1}); Drag: drag calculated from $F=6\pi\mu r U$, where r is derived from equivalent spherical diameter (ESD) in Table 1; NGD: net-to-gross displacement of swimming path; HPI: helical path index from $H=2\pi(a^2+b^2)^{1/2}$, where a is the helix and b is length of one helix cycle divided by 2π

Characteristic		*Proro* (a)	*Scripps* (b)	*Perid* (c)	*Gymno* (d)	*Gyro* I (e)	*Gyro* II (f)	*Gonyau* (g)
Sink. vel. (m d^{-1})								
Fluor	(1)	0.52 (0.10)	0.77 (0.17)	2.09 (0.38)	1.38 (0.31)	3.81 (0.25)	3.70 (0.19)	3.04 (0.38)
Fluor-n	(2)	0.45 (0.08)	1.54 (0.16)	1.66 (0.39)	ND	3.49 (0.15)	3.77 (0.18)	ND
Stokes	(3)	0.28 (0.12)	1.24 (0.29)	1.86 (0.38)	2.59 (0.52)	3.65 (0.88)	3.92 (0.62)	3.70 (0.86)
Stokes'-sf	(4)	0.26 (0.08)	1.24 (0.29)	1.79 (0.38)	2.40 (0.32)	3.65 (0.62)	3.93 (0.44)	3.72 (0.61)
Stokes'-n	(5)	0.37 (0.08)	1.44 (0.23)	2.00 (0.42)	ND	3.84 (0.59)	ND	ND
Video	(6)	ND	ND	ND	1.59 (2.38)	0.99 (5.20)	2.55 (3.04)	1.67 (4.51)
Video-n	(7)	0.51 (0.23)	1.32 (0.38)	1.87 (0.50)	ND	3.68 (1.03)	2.42 (0.68)	ND
Swim. vel. (m d^{-1})		14.8 (2.4)	13.2 (3.2)	16.0 (3.9)	11.7 (2.4)	28.5 (5.2)	26.3 (3.0)	22.3 (4.5)
Sink. Rey no. ($\times 10^{-5}$)		5	29	51	61	136	160	150
Swim. Rey no. ($\times 10^{-5}$)		194	318	458	420	1053	1048	874
Swim:sink		28.5 (7.2)	14.0 (3.8)	7.7 (2.3)	8.5 (2.6)	7.5 (1.5)	7.1 (0.9)	7.4 (1.8)
Approx rad (μm)		4.9 (0.7)	ND	8.0 (0.9)	24.5 (2.2)	13.1 (0.9)	ND	16.4 (1.6)
$\omega:U$ (rad μm^{-1})		0.110 (0.014)	ND	0.068 (0.009)	0.009 (0.002)	0.046 (0.005)	ND	0.016 (0.002)
Drag ($\times 10^{-6}$ dynes)		1.90	3.11	4.49	4.12	10.34	10.29	8.55
NGD		0.97 (0.03)	0.90 (0.09)	0.78 (0.13)	0.72 (0.24)	0.97 (0.03)	ND	0.67 (0.27)
HPI		0.94 (0.06)	0.81 (0.11)	0.73 (0.06)	0.75 (0.13)	0.96 (0.03)	ND	0.55 (0.18)

despite an eccentricity range between 0.50 and 0.87. A comparison of the "Stokes" and "Stokes'-n" rows (both calculated without the shape factor) in Table 2 identifies a larger but still limited difference when the densities of the narcotized (n) cells are substituted for those of the swimming cells. The various "Stokes" and "Fluor" determinations generally agreed within two standard deviations. The video approach works best on narcotized cells ("Video-n"), as shown by its general agreement with both the "Fluor" and "Stokes" approaches. The video determinations on swimming cells ("Video") were characterized by high standard deviations that severely limit the utility of this approach. In the subsequent discussions, the "Fluor" method on swimming cells will be used since it provides the most complete record of reliable sinking-velocity estimates. Fig. 1 clearly shows the strong dependence of sinking velocity on cell size represented as the square of the radius in Eq. (2).

Swimming velocity

The horizontal swimming-velocity determinations for the six dinoflagellates are given in Table 2. Because the computer analysis is based on 5 frames s^{-1} and because the swimming velocity is computed between considered frames, the swimming velocity approximates the helix velocity. The swimming velocities used here are compared at 20 °C and do not necessarily represent the absolute swimming-velocity maxima based on species-specific temperature responses as reported by Kamykowski and McCollum (1986). Swimming velocity did not exhibit a simple relationship with cell size.

Rotation : translation ratio and drag

The average ratio of rotation:translation velocity (ω/U) for each species is given in Table 2. The approximate equivalent spherical radii based on two cell dimensions ("Approx rad" in Table 2) represent different subpopulations than those used for the other measurements. The different rank order of cell size compared to the previously considered subpopulations demonstrates the temporal variability of average cell size within a species. The rotation : translation ratio tended to decrease with increasing cell size.

Drag is also recorded in Table 2. As expected from Eq. (5), drag tended to increase with cell size.

Path characteristics

The two-dimensional NGD and the three-dimensional HPI computed from Eq. (6) are also given in Table 2. These data and a graphically based, two-dimensional RCD (see "Discussion – Path characteristics") describe the character of paths. The NGD and HPI in Table 2 were closely related and decreased with increasing cell size, except for *Gyrodinium dorsum*.

Discussion

Density determinations

The differences between the density determinations on narcotized and swimming cells may be due to the deleterious effects of narcotization, which could cause cell shrinkage contributing to denser cells, but this effect would not necessarily be size-specific. Another more likely possibility is the differential effect of centrifugation shear on the swimming ability of the larger cells (Thomas and Gibson 1990) and the presence of a taxis (photo- or geo-) in the still motile smaller cells that contributes to the ascent to the overlying lower densities in the gradient during the course of the 10 min fractionation procedure. The actual cause of the discrepancies is not presently known, but the narcotized cell densities are considered more reliable.

Sinking velocity

The direct dependence of sinking velocity on cell size as stated in Eq. (2) is verified in Fig. 2A, which closely duplicates the log-based format used by Smayda (1970). The data for the dinoflagellate species measured in the present study (a–g in Fig. 2A), generally fall within the bounds of the two curves for healthy (lower) or senescent (upper) cells in Smayda's study. Fig. 2B compares the sinking-velocity determinations on the basis of the surface area:volume (SA:V) ratios using Smayda's log-based approach. The data for the dinoflagellate species measured in the present study generally fall between the two curves for maximum and minimum sinking velocities in Smayda's data. The new data extend the sinking-velocity coverage for dinoflagellates from that available to Smayda, and suggest that this class generally follows the geometric relationships that he derived based mainly on diatoms. The more precise determinations of dinoflagellate sinking velocities made in the present study can be used to assign ascent and descent swimming velocities where only horizontal swimming velocities are known, based on the concept in Eq. (3).

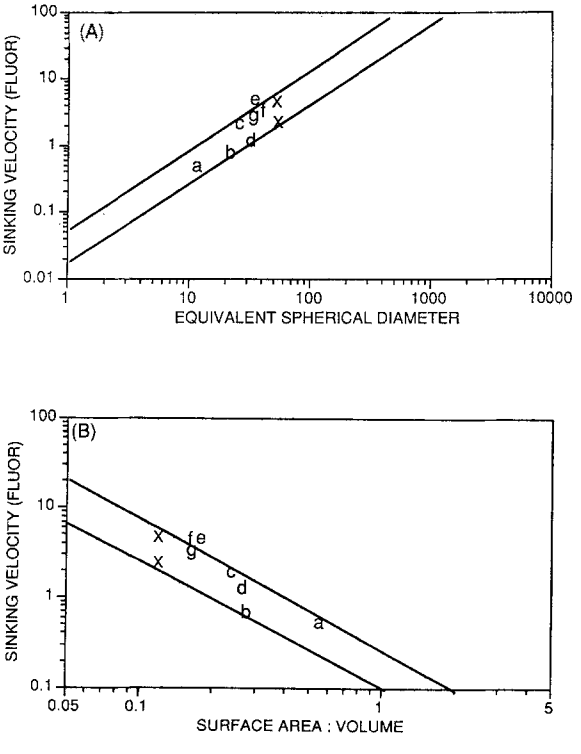

Fig. 2. *Prorocentrum mariae-lebouriae* (a), *Scrippsiella trochoidea* (b), *Peridinium foliaceum* (c), *Gymnodinium sanguineum* (d), *Gyrodinium dorsum* (e, f) and *Gonyaulax polyedra* (g). Scatter-plots of log sinking-velocity (Fluor; m d^{-1}) as a function of log equivalent spherical diameter (ESD; μm) (A) and log surface-area:volume (SA:V μm^{-1}) (B); abbreviations and data from Tables 2 and 1, respectively. In (A), "x" represents senescent (upper) and healthy (lower) cells of *Gonyaulax polyedra*, with upper and lower lines showing respective relationships (after Smayda 1970); in (B), upper and lower lines show maximum and minimum sinking velocities (m d^{-1}), respectively, for the single-cell species (after Smayda 1970)

Swimming velocity

The swimming velocities (Swim. vel.) recorded in the present study (0.5 to 1.2 m h^{-1}) fall in the range of those reported in the dinoflagellate literature, 0.03 to 6.5 m h^{-1} (Levandowsky and Kaneta 1987); most of the literature estimates fall below 1.3 m h^{-1}. The environmental sensitivity of swimming-velocity determinations on temperature, light intensity (Kamykowski et al. 1988) and probably other factors limits the usefulness of a more detailed external comparison. The uniform culture and measurement conditions used within the present study do support a consistent internal comparison among the selected species.

Surface area:volume

Sournia (1982) pointed out that SA:V often correlates well with physiological activity, since it permits and limits the exchange of energy and matter. Since sinking and swimming velocity are both functions of cell size (Happel and Brenner 1983), inverse relationships of SA:V with cell dimension are expected. Fig. 3A presents the previous data for dinoflagellate sinking velocity as a function of SA:V (Fig. 2B) on a linear scale. The dinokonts considered alone exhibited a strong relationship [$V_i = -22.90$ (SA:V) $+ 7.50$, $r^2 = 0.91$]. The desmokont deviated from this general trend and reduced the overall significance [$V_i = -7.79$ (SA:V) $+ 4.28$, $r^2 = 0.62$] when included with the dinokonts. This effect, however, may be due solely to the smaller size of the desmokont. The pattern for swimming velocity was similar to that of sinking velocity, with a stronger relationship for the dinokonts alone [$V_w = -125.99$ (SA:V) $+ 47.39$, $r^2 = 0.87$] than when the desmokont was included [$V_w = -27.72$ (SA:V) $+ 26.42$, $r^2 = 0.32$]. The difference in the swimming apparatus between dinokonts and desmokonts (different insertion points and lack of grooves) may weaken this relationship with SA:V when the desmokont is included, but the similar tendencies in Fig. 3A suggest that size again may be of primary importance. More measurements are required with small dinokonts to clarify the suggested relationships.

Reynolds numbers

Levandowsky and Kaneta (1987) discussed the application of Reynolds number (Eq. 4) to a variety of organisms. In general, Reynolds numbers < 0.1 characterize organisms that reside in a regime in which viscosity dominates (Granata and Dickey 1991). Levandowsky and Kaneta reported that the dinoflagellate *Dinophysis acuta*, with a length of < 50 µm and a swimming velocity of 43.2 m d^{-1}, corresponded to $Re < 0.02500$. Table 2 ("Sink. Rey no." and "Swim. Rey no.") lists Reynolds numbers for the sinking (0.00005 to 0.00150) or swimming (0.00194 to 0.01053) dinoflagellates in the present study that are smaller than Levandowsky and Kaneta estimated. The surveyed dinoflagellates definitely exist in the low Reynolds-number regime, and are thus affected by all of the attributes (Purcell 1977) related to dominant viscosity.

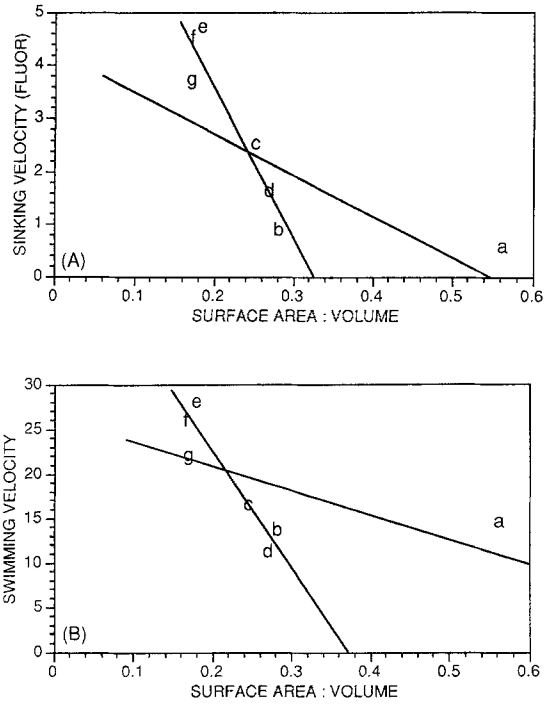

Fig. 3. *Prorocentrum mariae-lebouriae* (a), *Scrippsiella trochoidea* (b), *Peridinium foliaceum* (c), *Gymnodinium sanguineum* (d), *Gyrodinium dorsum* (e, f) and *Gonyaulax polyedra* (g). Scatter plots of sinking velocity (Fluor; m d^{-1}) (A) and swimming velocity (Swim. vel.; m d^{-1}) (B) as a function of surface area:volume (SA:V; µm^{-1}); abbreviations and data from Tables 2 and 1, respectively. In (A), more oblique regression line ($V_i = -22.90$ (SA:V) $+ 7.50$, $r^2 = 0.91$) represents dinokont relationship; less oblique regression line ($V_i = -7.79$ (SA:V) $+ 4.28$, $r^2 = 0.62$) represents desmokont plus dinokont relationship. In (B), dinokont relationship is given by $V_w = -125.99$ (SA:V) $+ 47.39$, $r^2 = 0.87$, while combined dinokont and desmokont regression is given by $V_w = -27.72$ (SA:V) $+ 26.42$, $r^2 = 0.32$

Swim:sink ratio

Based on laboratory data, Kamykowski et al. (1989) suggested that the ratio of swimming:sinking velocity (V_w:V_i) might influence the behavioral capabilities of different dinoflagellate species since sinking velocity adds to descent and subtracts from ascent (Roberts 1981). According to this relationship, species with a higher ratio should ascend and descend with equal ease; species with a lower ratio should descend more readily than ascend. The present analysis based on more precise determinations of sinking velocity and simultaneous determinations of swimming velocity yielded a different trend (Table 2) than that suggested by Kamykowski et al. (1989). Based on a literature survey, Sournia (1982) concluded that phytoflagellates generally swim ten times faster than they sink. Considering the desmokont and dinokonts combined, V_w:V_i decreased with increasing size from a high

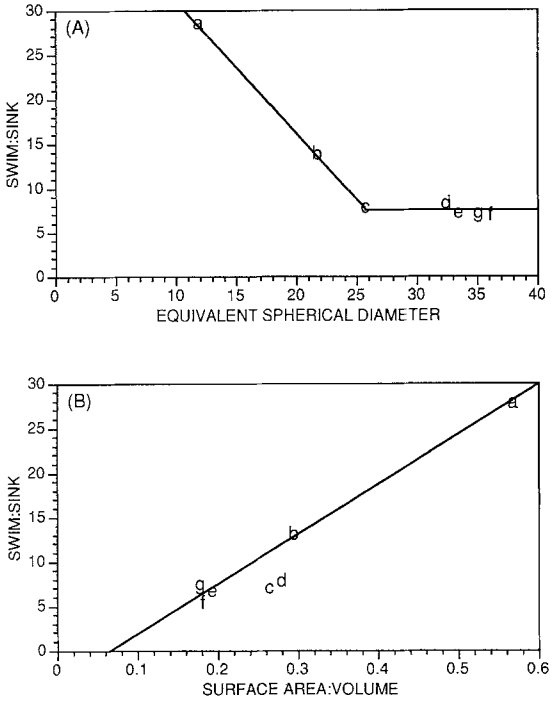

Fig. 4. *Prorocentrum mariae-lebouriae* (a), *Scrippsiella trochoidea* (b), *Peridinium foliaceum* (c), *Gymnodinium sanguineum* (d), *Gyrodinium dorsum* (e, f) and *Gonyaulax polyedra* (g). Scatter plots of ratio of swimming velocity:sinking velocity (Swim:sink) as a function of equivalent spherical diameter (ESD; μm) (A) and surface area:volume ratio (SA:V; μm^{-1}) (B); abbreviations and data from Tables 2 and 1, respectively. In (A), lines are eye fits to data; in (B), regression fit is $V_w : V_i = 55.50\,(SA:V) - 3.40$, $r^2 = 0.93$

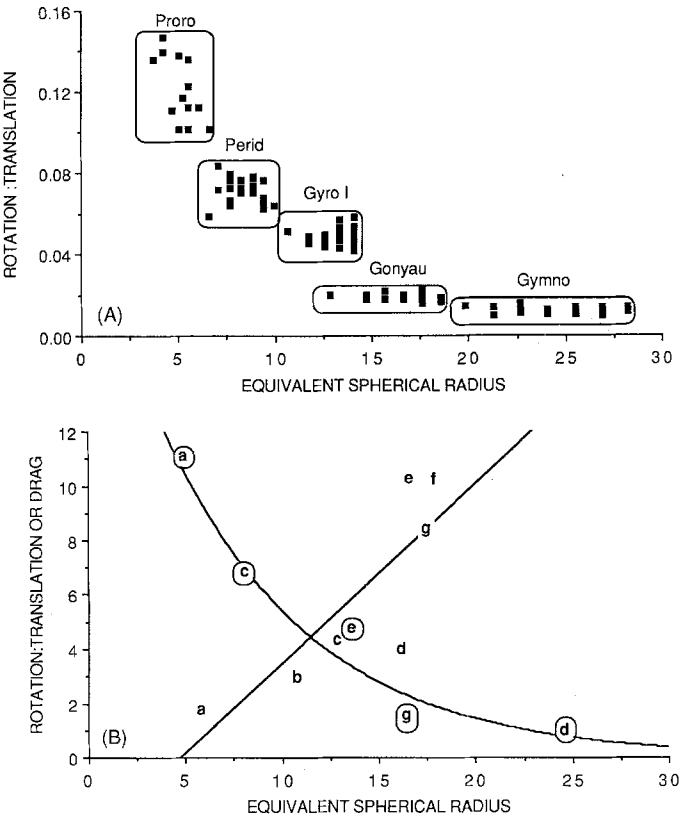

Fig. 5. *Prorocentrum mariae-lebouriae* (*Proro*; a) *Scrippsiella trochoidea* (b), *Peridinium foliaceum* (*Perid*; c), *Gymnodinium sanguineum* (*Gymno*; d), *Gyrodinium dorsum* (*Gyro* I and II; e) and *Gonyaulax polyedra* (*Gonyau*; f). (A) Scatter plots of rotation:translation velocity ($\omega:U$; rad μm^{-1}) as a function of approximate equivalent spherical radius (Approx rad; μm) for all cells examined. (B) Scatter plots of rotation:translation velocity ($\times 10^{-2}$ rad μm^{-1}; circled letters) fit by $\omega:U = 20.21\ e^{-0.1319r}$ ($r^2 = 0.94$) for species' means in (A) as a function of approximate equivalent spherical radius and of drag ($\times 10^{-6}$ dynes; uncircled letters) fit by $F = 0.66\,r - 3.12$ ($r^2 = 0.69$) as a function of equivalent spherical radius (ESD/2 from Table 1; μm); abbreviations and data from Table 2 unless otherwise stated

value of 28.5 at an ESD of 11.7 μm to a constant value averaging 7.6 above ESDs of 25 μm (Fig. 4A). Applying the concept expressed by Eq. (3), the smallest cell considered ascends at 93% of the velocity at which it descends, while cells >25 μm in diameter ascend only 75% as fast as they descend. Fig. 4B shows that the $V_w : V_i$ values for the desmokont and dinokonts considered together were linearly related to the SA:V ratios [$V_w : V_i = 55.50\,(SA:V) - 3.40$, $r^2 = 0.93$].

Size-dependence of swimming velocity

Fig. 5A expands the interpretation of the average rotation:translation ratio ($\omega:U$) in Table 2 by displaying the actual cell-specific data for each species. Surprisingly, the five species measured did not overlap, although they were not chosen on this basis. Note that if the boundaries marking each species' subregion were removed, the data would suggest an exponential decay of rotation:translation with increasing approximate ESD (r). Fig. 5B quantifies this relationship [$\omega:U = 20.21\ e^{-0.1319r}$; $r^2 = 0.94$] based on the averages of $\omega:U$ in Table 2. This empirical relationship agrees with hydrodynamic theory (Roberts 1981) and supports the explanation of decreasing swimming velocity at ESDs below ~35 μm (Kamykowski and McCollum 1986). Fig. 5B also reveals the linear increase of drag ("Drag" in Table 2), with increasing cell size for the same subpopulations that provided the swimming velocity estimates. Drag (F) increased with ESD (r) as $F = 0.66\,r - 3.12$ ($r^2 = 0.69$). This relationship supports the explanation of decreasing swimming velocity at ESDs, above ~35 μm by Kamykowski and McCollum. The two relationships in Fig. 5B thus combine to support the hypothesis of an intermediate cell size for the maximum swimming velocity based on an assumed standard dinoflagellate-propulsion system. This relationship, however, requires further testing since swimming velocity (U) generally increases with cell length [represented by L in Eq. (7) for clarity] at least when organisms spanning nine

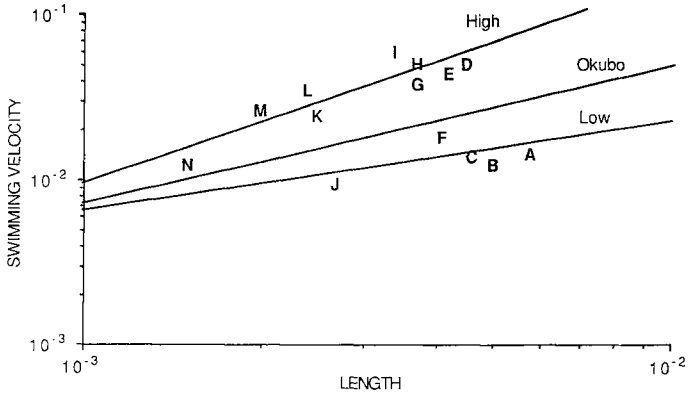

Fig. 6. A: *Gymnodinium splendens* (also known as *G. sanguineum*); B: *Prorocentrum micans*, Clone L313; C: *P. micans*, Clone 1993; D: *Protoceratium reticulatum;* E: *Gonyaulax polyedra*, Clone GP60e; F: *Prorocentrum micans*, Clone Proro III; G: *G. polyedra*, Clone Py-70A; H: *Gyrodinium dorsum;* I: *Peridineum foliaceum;* J: *Gymnodinium nelsonii;* K: *Amphidinium carterae;* L: *Cachonina illdefina;* M: *C. niei;* N: *Glenodinium* sp. Scatter-plot of swimming velocity (cm s^{-1}) as a function of cell length (cm) for dinoflagellates by Kamykowski and McCollum (1986), and using their species designations. Middle line represents $U = 2.69\ L^{0.86}$ from Okubo (1987), where U = swimming velocity and L = organism length; upper line, $U = 30.66\ L^{1.16}$ ($r^2 = 0.79$) for species above middle line; lower line, $U = 0.16\ L^{0.46}$ ($r^2 = 0.32$) for species below middle line

orders of magnitude in size are considered (Okubo 1987). Fig. 6 compares Okubo's relationship:

$$U = 2.69\ L^{0.86}, \tag{7}$$

as applied to the dinoflagellate size range with the dinoflagellate data from Kamykowski and McCollum. The data are divided into two groups by Okubo's relationship. Of the nine genera considered, seven are included in the upper group represented by $U = 30.66\ L^{1.16}$ ($r^2 = 0.79$) and two, *Prorocentrum* and *Gymnodinium*, are included in the lower group represented by the weaker relationship $U = 0.16\ L^{0.46}$ ($r^2 = 0.32$). This analysis supports an alternate hypothesis that swimming velocity generally increases with cell size, but that different dinoflagellate genera follow different trends with cell size that may be related to differences in their specific expression of a basic dinoflagellate-propulsion system. Considering all of the dinoflagellate genera together, Okubo's relationship (Eq. 7) provides a good qualitative representation of the group. More observations are required to distinguish between these and other possible hypotheses.

Path characteristics

Fig. 7 displays representative paths for each of the species, and demonstrates that the motion contributing to intermediate NGD values is more complicated than that suggested by the description of the extremes (see "Materials and methods" – Path characteristics). The panels are arranged from left to right, then top to bottom, in order of decreasing NGD. All the species examined exhibited some degree of helical swimming. The species with the higher NGD values tended to describe helices in which the radius was relatively small (~20%) compared to the length of one helix cycle. Species with lower NGD values tended to describe helices in which the radius was larger (>40%) than the length of one helix cycle. The three dimensional HPI provides a direct measure of each species' swimming ability if a mean direction is maintained. It was clearly related to the two-dimensional NGD, but did not take abrupt changes in mean direction into account. Although helical features are evident in the path described by *Gymnodinium sanguineum*, this species appears to change its mean direction more frequently than the other species studied.

Fig. 7 also displays the histograms of the RCD, the third path trajectory characteristic. The similarity of this diagnostic for *Porocentrum mariae-lebouriae* and *Gyro-*

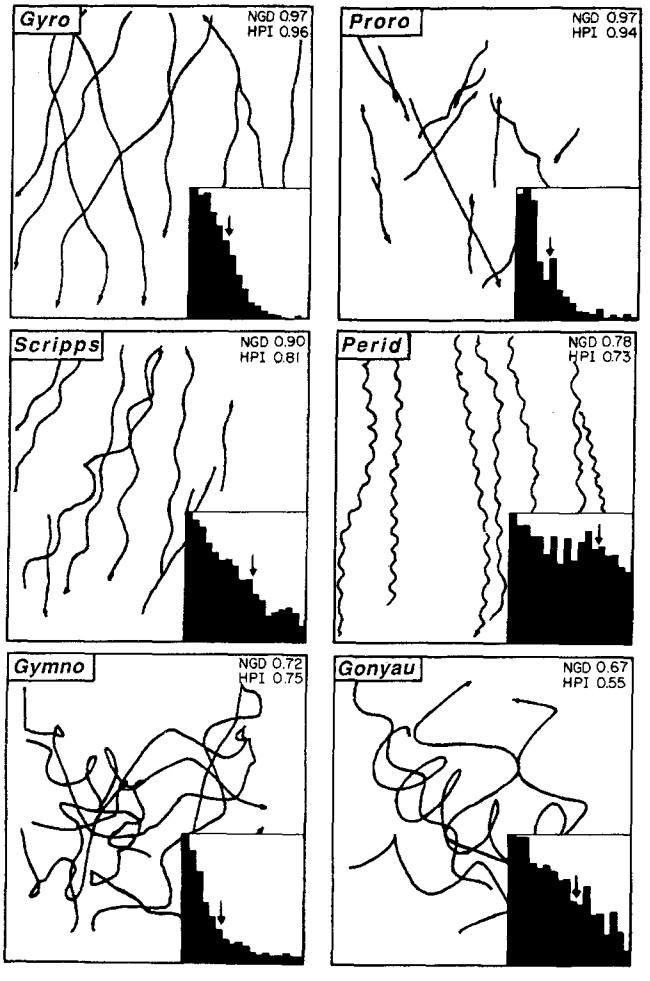

Fig. 7. *Prorocentrum mariae-lebouriae* (*Proro*), *Scrippsiella trochoidea* (*Scripps*), *Peridinium foliaceum* (*Perid*), *Gymnodinium sanguineum* (*Gymno*), *Gyrodinium dorsum* (*Gyro* I and II) and *Gonyaulax polyedra* (*Gonyau*). Representative, two-dimensional cell trajectories as produced by motion-analysis system for six marine dinoflagellates. Presented from left to right and then top to bottom in order of decreasing net-to-gross displacement (NGD). Numbers in upper right corner of each plot show species' NGD and helical path index (HPI), respectively. Histograms in lower right of each plot show rate-of-change-of-direction diagnostic scaled from 0° (left) to 180° (right). Arrows mark 75% distribution above each histogram

dinium dorsum on the one hand and for *Scrippsiella trochoidea*, *Peridinium foliaceum*, and *Gonyaulax polyedra* on the other hand suggests a sensitivity to the characteristics of the helical paths. In this case, however, *Gymnodinium sanguineum* is more like *Gyrodinium dorsum* and *Prorocentrum mariae-lebouriae*. The unique motion of *Gymnodinium sagnuineum* apparently requires both computer-derived, two-dimensional indices to properly distinguish it from the simple patterns of the other species.

The swimming-velocity measurements presented by Kamykowski et al. (1988) as measured with the "Expertvision" motion-analysis system are really estimates of the helix velocity (see "Results – Swimming velocity"). The two-dimensional NGD or the three-dimensional HPI provide a correction that can be applied to individual species to model their actual translation velocity. For example, *Gonyaulax polyedra* swims at a helical velocity of 22.3 m d^{-1} (Table 2) or 258 μm s^{-1}. An NGD of 0.67 or an HPI of 0.55 yield translation velocities of 173 or 142 μm s^{-1}, respectively. If these three rates are compared as a descent from the surface over a 12 h period, the relative depths attained are 11.1, 7.5 and 6.1 m, respectively. The actual translation velocity can make a significant difference in the vertical progress of a given species and thus to its ability to cope with an energetic environment. The three-dimensional HPI conceptually appears to offer the best correction. A remaining question is how the helix geometry changes with realistic environmental conditions as developed in field-oriented biophysical models (Yamazaki and Kamykowski 1990).

Acknowledgements. This material is based upon work supported by the National Science Foundation under Grant No. OCE 8818292. We thank the PAMS shop under Mr. J. Johnson for expeditiously providing the required fabrications and Ms. L. Salzillo for drafting assistance. Discussions with Dr. G. S. Janowitz and the NCSU Statistics Department and the suggestions of the reviewers and editor contributed to the presentation

Literature cited

Bailey, T. G. (1975). Chemical composition of two species of nitrate- and phosphate-deficient marine dinoflagellates. M. S. thesis. University of California, Santa Barbara

Bienfang, P., Laws, E., Johnson, W. (1977). Phytoplankton sinking rate determination: technical and theoretical aspects, an improved methodology. J. exp. mar. Biol. Ecol. 30:283–300

Bovee, E. C. (1982). Movement and locomotion of *Euglena*. In: Buetow, D. E. (ed.) The biology of *Euglena*. Vol. 3 Academic Press, New York, p. 143–168

Brennen, C., Winet, H. (1977). Fluid mechanics of propulsion by cilia and flagella. A. Rev. Fluid Mech. 9:339–398

Cox, E. R. (1980). Phytoflagellates. Elsevier/North Holland, New York

Crenshaw, H. (1990). An introduction to the kinematics of helical motion. Lecture Notes Biomaths 89:362–386

Eppley, R. W., Holmes, R. W., Strickland, J. D. H. (1967). Sinking rates of marine phytoplankton measured with a fluorometer. J. exp. mar. Biol. Ecol. 1:191–208

Granata, T. C., Dickey, T. D. (1991). The fluid mechanics of copepod feeding in a turbulent flow: A theoretical approach. Prog. Oceanogr. 26:243–261

Happel, J., Brenner, H. (1983). Low Reynolds number hydrodynamics. Martinus Nijhoff, The Hague

Kamykowski, D., McCollum S. A. (1986). The temperature acclimatized swimming speed of selected marine dinoflagellates. J. Plankton Res. 8:275–287

Kamykowski, D., McCollum, S. A., Kirkpatrick G. J. (1988). Observations and a model concerning the translational velocity of a photosynthetic marine dinoflagellate under variable environmental conditions. Limnol. Oceanogr. 33:66–78

Kamykowski, D., McCollum, S. A., Kirkpatrick G. (1989). A comparison of the environmentally modulated swimming behavior of several photosynthetic marine dinoflagellates. In: Okaichi, T. et al. (eds.) Red tides: biology, environmental science, and toxicology. Elsevier Science Publishing Co., New York, p. 277–280

Levandowsky, M., Kaneta, P. (1987). Behaviour in dinoflagellates. In: Taylor, F. J. R. (ed.) The biology of dinoflagellates. Blackwell Scientific Publications, Oxford, p. 360–398

Lindholm, T. (1982). EDTA and oxalic acid – two useful agents for narcotizing fragile and rapid microzooplankton. Hydrobiologia 86:297–298

McNown, J. S., Malaika, J. (1950). Effects of particle shape on settling velocity at low Reynolds numbers. Trans. Am. geopyhs. Un. 31:74–82

Okubo, A. (1987). The fantastic voyage into the deep: marine biofluid mechanics. Biomaths. 71:32–47

Omori, M., Ikeda, T. (1984). Methods in marine zooplankton ecology. John Wiley & Sons, New York

Parsons, T. R., Maita, Y., Lalli, C. M. (1984). A manual of chemical and biological methods for seawater analysis. Pergamon Press, Oxford

Peters, N. (1929). Orts- und Geisselbewegung bei marinen Dinoflagellaten. Arch. Protistenk. 67:291–321

Price, C. A. (1972). Centrifugation in density gradient. Academic Press, New York

Purcell, E. M. (1977). Life at low Reynolds number. Am. J. Phys. 45:3–11

Rees, C. E. (1984). Error propagation calculations. Geochim. cosmochim. Acta 48:2309–2311

Reize, I. B., Melkonian, M. (1989). A new way to investigate living flagellated-ciliated cells in the light microscope: immobilization of cells in agarose. Botanica Acta (Ber. dt. bot. Ges.) 102:145–151

Roberts, A. M. (1981). Hydrodynamics of protozoan swimming. In: Levandowsky, H.; Hutner, S. H. (eds.) Biochemistry and physiology of protozoa. Vol. 4. Academic Press, New York, p. 5–66

Salas, S. L., Hille, E. (1974). Calculus: one and several variables. John Wiley & Sons, New York

SAS Institute Inc. (1985). SAS user's guide: statistics. Version 5 edn. SAS Institute Inc., Cary, North Carolina

Selby, S. M. (1965). Standard mathematical tables. 14th ed. The Chemical Rubber Co., Cleveland, Ohio

Smayda, T. J. (1970). The suspension and sinking of phytoplankton in the sea. Oceanogr. mar Biol. A. Rev. 8:353–414

Sournia, A. (1982) Form and function in marine phytoplankton. Biol. Rev. 57:347–394

Taylor, F. J. R., Pollingher, U. (1987). Ecology of dinoflagellates. In: Taylor, F. J. R. (ed.) The biology of dinoflagellates. Blackwell Scientific Publications, Oxford, p. 399–529

Thomas, W. H., Gibson, C. H. (1990). Effects of small-scale turbulence on microalgae. J. appl. Phycol. 2:71–77

U.S. Navy Oceanographic Office. (1966). Handbook of oceanographic tables. U.S. Navy Oceanographic Office, Washington, D. C. (Spec. Publ. No. 68)

Van Ierland, E. T., Peperzak, L. (1984). Separation of marine seston and density determination of marine diatoms by density gradient centrifugation. J. Plankton Res. 6:29–44

Yamazaki, H., Kamykowski, D. (1990). The vertical trajectories of motile phytoplankton in a wind-mixed water column. Deep-Sea Res. 38:219–241